Letm1, the mitochondrial Ca^{2+}/H^{+} antiporter, is essential for normal glucose metabolism and alters brain function in Wolf–Hirschhorn syndrome

Dawei Jiang[a,b,c], Linlin Zhao[a,b,c], Clary B. Clish[d], and David E. Clapham[a,b,c,1]

[a]Department of Cardiology, Howard Hughes Medical Institute, [b]Manton Center for Orphan Disease, Children's Hospital Boston, and [c]Department of Neurobiology, Harvard Medical School, Boston, MA 02115; and [d]Broad Institute of Massachusetts Institute of Technology and Harvard University, Cambridge, MA 02142

Contributed by David E. Clapham, May 6, 2013 (sent for review February 18, 2013)

Mitochondrial metabolism, respiration, and ATP production necessitate ion transport across the inner mitochondrial membrane. Leucine zipper-EF-hand containing transmembrane protein 1 (*Letm1*), one of the genes deleted in Wolf–Hirschhorn syndrome, encodes a putative mitochondrial Ca^{2+}/H^{+} antiporter. Cellular Letm1 knockdown reduced $Ca^{2+}{}_{mito}$ uptake, $H^{+}{}_{mito}$ extrusion and impaired mitochondrial ATP generation capacity. Homozygous deletion of *Letm1* in mice resulted in embryonic lethality before day 6.5 of embryogenesis and ∼50% of the heterozygotes died before day 13.5 of embryogenesis. The surviving heterozygous mice exhibited altered glucose metabolism, impaired control of brain ATP levels, and increased seizure activity. We conclude that loss of Letm1 contributes to the pathology of Wolf–Hirschhorn syndrome in humans and may contribute to seizure phenotypes by reducing glucose oxidation and other specific metabolic alterations.

calcium signaling | mitochondria | epilepsy

Mitochondria are major effectors and regulators of intracellular $[Ca^{2+}]$. Calcium-mediated signal transduction across the inner mitochondrial membrane (IMM) links increased metabolic demand to ATP production rate because Ca^{2+} regulates key metabolic enzymes, metabolite transporters, and the F_1F_0 H^{+}-ATPase (1, 2). Excessive Ca^{2+} accumulation reduces mitochondrial membrane potential ($\Delta\Psi_{mito}$), impairs ATP production, precipitates phosphate, and triggers cell death. Ca^{2+} extrusion across the IMM represents a significant energy cost at normal $\Delta\Psi_{mito}$ (∼−180 mV) and thus mitochondrial Ca^{2+} ($Ca^{2+}{}_{mito}$) signaling is tightly controlled under physiological conditions (3–5).

The mitochondrial Ca^{2+} uniporter (MCU), a highly Ca^{2+}-selective channel (6), dominates fast $Ca^{2+}{}_{mito}$ uptake when $[Ca^{2+}]_{cyto}$ is high, significantly buffers extramitochondrial Ca^{2+}, and depolarizes $\Delta\Psi_{mito}$ (7, 8). Because the MCU's V_{max} is orders of magnitude higher than that of $Ca^{2+}{}_{mito}$ exchange mechanisms, repetitive high $Ca^{2+}{}_{cyto}$ elevations trigger $Ca^{2+}{}_{mito}$ overload and can lead to the mitochondrial permeability transition (9, 10). Free $[Ca^{2+}]_{mito}$ in intact cells usually fluctuates below the micromolar range, suggesting that Ca^{2+} exchangers are crucial for maintaining $Ca^{2+}{}_{mito}$ homeostasis at low $Ca^{2+}{}_{cyto}$ levels to preserve mitochondrial homeostasis and bioenergetics. The Na^{+}/Ca^{2+} exchanger, Ca^{2+}/H^{+} antiporter, and potentially others, control Ca^{2+} across the IMM. Mitochondrial transporters and channels are rapidly being identified (11).

We previously performed a genome-wide RNAi screen in *Drosophila* S2 cells that identified Letm1 (leucine zipper-EF-hand containing transmembrane protein 1) as a mitochondrial Ca^{2+}/H^{+} antiporter (12). Letm1 is an evolutionarily conserved, ubiquitously expressed IMM protein. Heterozygous deletion of a chromosomal region containing *Letm1* is associated with Wolf–Hirschhorn syndrome (WHS), a disease characterized by craniofacial defects, growth and mental retardation, muscle hypotonia, congenital heart defects, and seizures (13). In the current study, we generated Letm1-deficient mice and found that Letm1 knockdown reduced $Ca^{2+}{}_{mito}$ uptake at low $[Ca^{2+}]_{cyto}$, impaired mitochondrial ATP generation capacity, disrupted early embryonic development, altered glucose metabolism, and increased susceptibility to seizures. These results are consistent with the WHS seizure phenotype in humans and show that Letm1 alters mitochondrial energetic performance and metabolic pathways.

Results

Letm1 Regulates $[Ca^{2+}]_{mito}$ and $[H^{+}]_{mito}$ Homeostasis and Mitochondrial Energetics. In initial experiments, Letm1 was transiently reduced using siRNAs to investigate short-term responses to protein loss and mitigate long-term developmental or compensatory mechanisms. Letm1 knockdown by RNA interference in Flp-In-293 cells resulted in dramatically reduced $Ca^{2+}{}_{mito}$ uptake in low $[Ca^{2+}]_{cyto}$ that was coupled with $H^{+}{}_{mito}$ extrusion (Fig. 1*A*). Na^{+}-dependent $Ca^{2+}{}_{mito}$ extrusion, mediated by the Na^{+}/Ca^{2+} exchanger, balances steady-state $[Ca^{2+}]_{mito}$ levels in low $[Ca^{2+}]_{cyto}$; a dramatically reduced steady-state $[Ca^{2+}]_{mito}$ was measured in Letm1 knockdown cells in the presence of 10 mM Na^{+}. In contrast, high $[Ca^{2+}]_{cyto}$ triggered a fast $[Ca^{2+}]_{mito}$ rise in cells with Letm1 knockdown to a level similar to that in controls (Fig. 1*A*). These results suggest that Letm1 is crucial for $Ca^{2+}{}_{mito}$ homeostasis in low $[Ca^{2+}]_{cyto}$.

Constant H^{+} pumping by the electron transport chain (ETC) establishes a highly negative membrane potential across the mitochondrial inner membrane. Cells in which Letm1 was knocked down (Fig. 1*B*) resulted in similar or slightly higher tetramethylrhodamine methyl ester (TMRM) accumulation (Fig. 1*C*), consistent with minimal changes in mitochondrial membrane potential. Certain populations of mitochondria with increased volume can be identified in Letm1 knockdown cells, but

Significance

Wolf–Hirschhorn syndrome (WHS), caused by deletions in 4p16.3, was the first recognized subtelomeric deletion syndrome. As with other syndromes of this class, WHS has not yet been subjected to an intensive, systematic analysis using mouse or cellular models. We recently identified leucine zipper-EF-hand containing transmembrane protein 1 (Letm1) as a mitochondrial Ca^{2+}/H^{+} antiporter, located in the core WHS region. In this study, *Letm1* null mice were generated and characterized. Deletion of *Letm1* disrupts early embryonic development, reduces glucose oxidation and thus particularly affects brain function.

Author contributions: D.J. and D.E.C. designed research; D.J. and L.Z. performed research; D.J., L.Z., and C.B.C. contributed new reagents/analytic tools; D.J., L.Z., and C.B.C. analyzed data; and D.J., C.B.C., and D.E.C. wrote the paper.

The authors declare no conflict of interest.

[1]To whom correspondence should be addressed. E-mail: dclapham@enders.tch.harvard.edu.

This article contains supporting information online at www.pnas.org/lookup/suppl/doi:10.1073/pnas.1308558110/-/DCSupplemental.

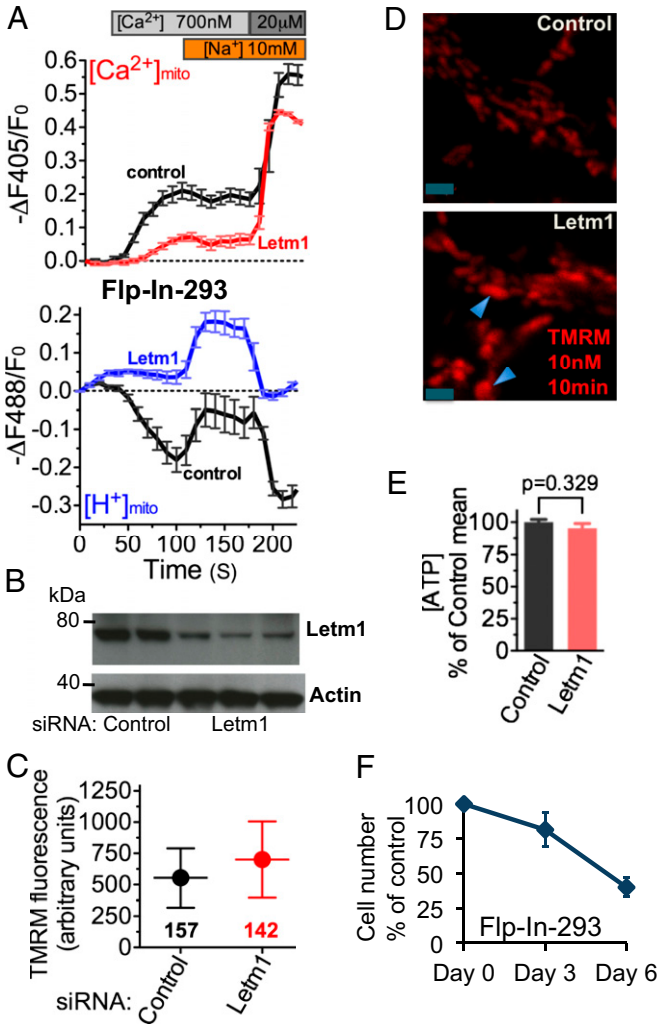

Fig. 1. Letm1 knockdown reduces $[Ca^{2+}]_{mito}$ and $[H^+]_{mito}$, but has minor effects on $\Delta\Psi_{mito}$. (*A*) $[Ca^{2+}]_{mito}$ and $[H^+]_{mito}$ measured by mt-pericam in digitonin-permeabilized Flp-In-293 cells treated with control (n = 4) or Letm1 siRNAs (n = 4) for 4 d. Traces shown are the mean mitochondrial signals from the whole imaging field. Ca^{2+} and Na^+ were applied as indicated. (*B*) Letm1 protein levels in Flp-In-293 cells treated with control siRNAs (left two lanes) or Letm1 siRNAs (right three lanes from three independent experiments) analyzed by Western blotting. (*C*) Plots of TMRM measurements of $\Delta\Psi_{mito}$ in control and Letm1 siRNA-treated Flp-In-293 cells (mean ± SD). (*D*) Images showing TMRM-labeled mitochondria following siRNA treatment for 4 d. Blue arrowheads denote enlarged mitochondria. (Scale bar, 2 μm.) (*E*) [ATP] of FLP-In-293 cells treated with *Letm1* siRNA for 4 d normalized to control cells (n = 3). (*F*) Percent of surviving FLP-In-293 cells treated with *Letm1* siRNA for 6 d normalized to control cells (n = 3).

they accumulated TMRM normally (Fig. 1*D*). Transient Letm1 knockdown did not result in a dramatically reduced total cellular [ATP] in Flp-In-293 cells (Fig. 1*E*). However, cell proliferation rates were progressively reduced in cells with long-term Letm1 knockdown (Fig. 1*F*). We postulate that Letm1 knockdown impairs cell proliferation, likely by affecting signaling pathways related with mitochondrial metabolism.

Letm1 Is Essential for Early Embryonic Development. To study the function of Letm1 in vivo, two independent gene-trap mouse lines lacking the *Letm1* gene were generated (Fig. S1 *A* and *B*). Full-length mRNA levels were reduced by ~50% in $Letm1^{+/-}$ mice, confirming the effectiveness of this strategy. $Letm1^{-/-}$ pups could not be obtained by crossing $Letm1^{+/-}$ heterozygotes, suggesting that homologous deletion of *Letm1* is embryonically lethal (Fig. S1*C*). Mendelian ratios of littermate genotypes indicated that approximately half of the $Letm1^{+/-}$ mice died before birth. We isolated and analyzed embryos from $Letm1^{+/-}$ intercrosses at various times after fertilization and determined that $Letm1^{-/-}$ embryos died before day 6.5 of embryogenesis (E6.5) and ~50% of the $Letm1^{+/-}$ embryos died before E13.5 (Fig. 2*A*). These results suggest a *Letm1* gene dosage effect on early embryonic development and survival.

E9.5 $Letm1^{+/-}$ embryos were growth-retarded (Fig. 2*B*), with a reduced rate of DNA synthesis (BrdU incorporation), but exhibited no significant increase in apoptosis (Fig. 2*C*). Developing embryos use significantly more ATP in support of rapid growth and differentiation; [ATP] in E9.5 embryos was ~10-fold higher than in adult differentiated tissues (Fig. 2*D*). We speculate that early $Letm1^{+/-}$ embryogenesis is compromised due to reduced ATP generation capacity, a defect with variable penetrance that can be partially compensated by glycolysis.

After the critical stages of early embryogenesis, surviving E13.5 $Letm1^{+/-}$ embryos seem grossly normal (Fig. 3*A*). Mitochondrial morphology and $\Delta\Psi_{mito}$ in cultured primary fibroblasts from $Letm1^{+/-}$ embryos were similar to WT (Fig. 3 *B*–*D*). Primary fibroblasts from $Letm1^{+/-}$ embryos had reduced $Ca^{2+}{}_{mito}$ uptake rates, low steady-state $[Ca^{2+}]_{mito}$, and reduced matrix pH compared with WT (Fig. S2*A*). O_2 consumption rates were similar in fibroblasts grown in high-glucose media with pyruvate supplement

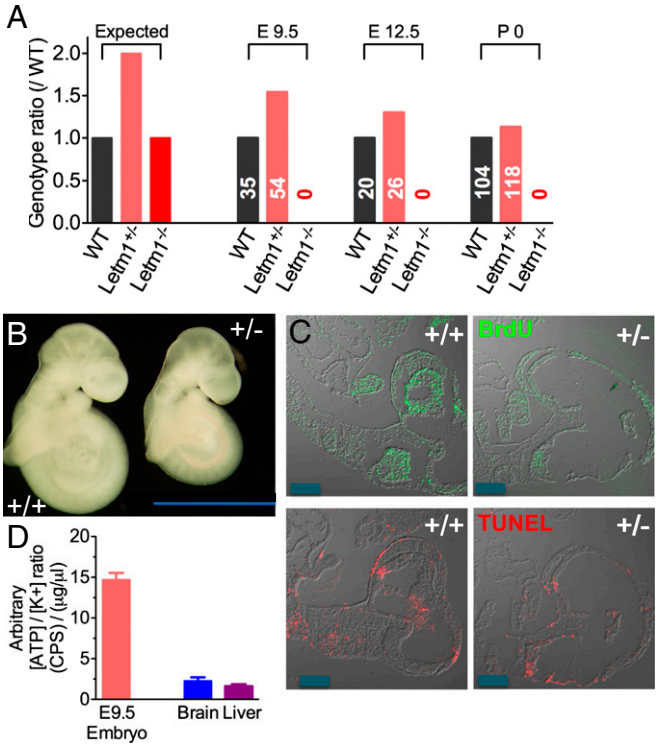

Fig. 2. Genetic deletion of Letm1 dramatically reduces mouse embryonic survival. (*A*) Percentage of embryos or mice with the indicated genotype at different development stages from $Letm1^{+/-}$ intercrosses. (*B*) Representative images of WT (*Left*) and $Letm1^{+/-}$ mouse embryos at E9.5. (Scale bar, 2 mm.) (*C*) BrdU and TUNEL staining in E9.5 *wt* and $Letm1^{+/-}$ mouse embryos indicates decreased BrdU incorporation but no significant apoptosis. (Scale bar, 200 μm.) (*D*) Luciferase-based tissue [ATP] measurements (cps) were normalized to $[K^+]$ (μg/μL) of the same sample by ICP-MS analysis. This normalization provides a comparison of total ATP content among various tissues, assuming similar tissue $[K^+]$. Samples analyzed were from WT E9.5 embryos (n = 5), brain (n = 4), and liver (n = 4) tissues from 6-wk-old mice.

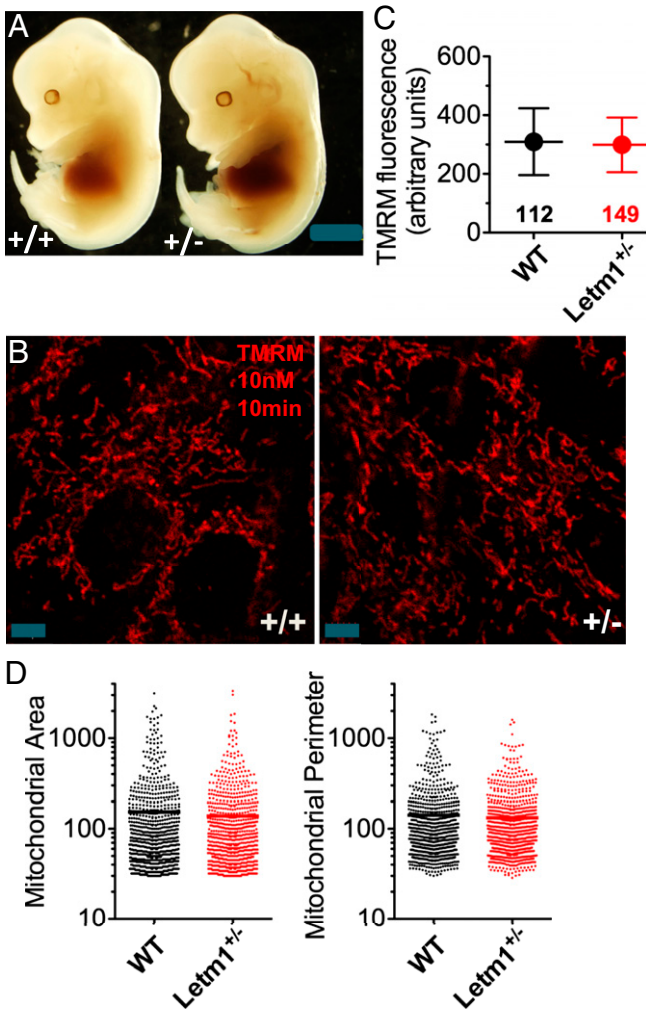

Fig. 3. Mitochondrial morphology and $\Delta\Psi_{mito}$ in primary fibroblasts. (*A*) Representative images of WT (*Left*) and *Letm1*$^{+/-}$ mouse embryos at E13.5. (Scale bar, 2 mm.) (*B*) Images showing TMRM-labeled mitochondria in primary fibroblasts isolated from WT and *Letm1*$^{+/-}$ E13.5 embryos. (Scale bar, 5 μm.) (*C*) TMRM measurements show no diference in $\Delta\Psi_{mito}$ in WT and *Letm1*$^{+/-}$ fibroblasts (mean ± SD). (*D*) Mitochondrial area and perimeter, as measured from electron microraphs (Fig. S3*A*), are comparable between WT and *Letm1*$^{+/-}$ fibroblasts. Each point is the analysis of one mitochondrial area; n = 847 for WT and 901 for *Letm1*$^{+/-}$.

(to provide saturating oxidation substrates), consistent with normal ETC function (Fig. S2*B*). However, both basal and maximum O_2 consumption rates were reduced in *Letm1*$^{+/-}$ fibroblasts grown in low-glucose medium, suggesting that Letm1 is important for efficient glucose oxidation in mitochondria (Fig. S2*B*).

Because WHS is caused by a heterozygous subtelomeric deletion, we reasoned that *Letm1*$^{+/-}$ heterozygous mice better mimic this genetic defect than homozygous knockout mice. *Letm1*$^{+/-}$ mice that were born seemed grossly normal without facial or midline developmental defects (Fig. 4*A*) despite detectable Letm1 protein reduction (Fig. 4*B*). *Letm1*$^{+/-}$ mice have body weights similar to those of WT mice at 6 wk after birth (Fig. 4*C*). Under resting conditions in *Letm1*$^{+/-}$ mice, heart size, as calibrated in the heart/body weight ratio, was modestly reduced (Fig. 4*C*).

Letm1 Deficiency Impairs Brain [ATP] Regulation. There were no obvious general mitochondrial alterations or histological defects detected in *Letm1*$^{+/-}$ mice. Mitochondrial morphology was intact in *Letm1*$^{+/-}$ tissues (Fig. S3*A*) and under normal feeding conditions, the heart, liver, and brain [ATP] were all similar in *Letm1*$^{+/-}$ and WT mice (Fig. S3*B*). However, a 27% reduction in brain [ATP] (P = 0.013) was observed after 48 h of fasting, whereas liver and heart [ATP] were not significantly altered (Fig. 4*D* and Fig. S3*C*). In contrast to heart and liver, the brain cannot oxidize fatty acids and preferentially uses glucose as the energy substrate for mitochondrial oxidative phosphorylation. Indeed, the activity of pyruvate dehydrogenase, the key rate-limiting Ca^{2+}-sensitive enzyme that controls glucose oxidation, was significantly reduced in *Letm1*$^{+/-}$ brain (Fig. 4*E*). The heart is also influenced by mitochondrial ETC dysfunction and fatty acid oxidation (14), but the measured [ATP] in *Letm1*$^{+/-}$ hearts indicates that fatty acid oxidation in mitochondria and the ETC is not significantly altered at rest. Taken together, the results suggest a tissue-dependent alteration of energy metabolism in *Letm1*$^{+/-}$ mice, most likely due to the differential impact of Letm1 on mitochondrial metabolic pathways.

Letm1 Deficiency Disrupts Glucose Metabolism. To investigate how Letm1 deficiency affects tissue metabolism, we performed high-throughput metabolic profiling of tissues from *Letm1*$^{+/-}$ and WT mice. Approximately 200 intracellular metabolic intermediates were measured using liquid chromatography-mass spectrometry (LC-MS) (15, 16). Increases in key glycolysis intermediates were seen, consistent with a decrease in mitochondrial ATP generation capacity (Fig. 5). In addition, we observed altered tryptophan metabolism in *Letm1*$^{+/-}$ brain tissue, likely related to the amino acid salvage pathways that are part of acetyl-CoA and nicotinamide synthesis (Fig. 5). Key intermediates of the tricarboxylic acid (TCA) cycle (e.g., succinate, malate, and fumarate) were not affected, indicating normal ETC function. Interestingly,

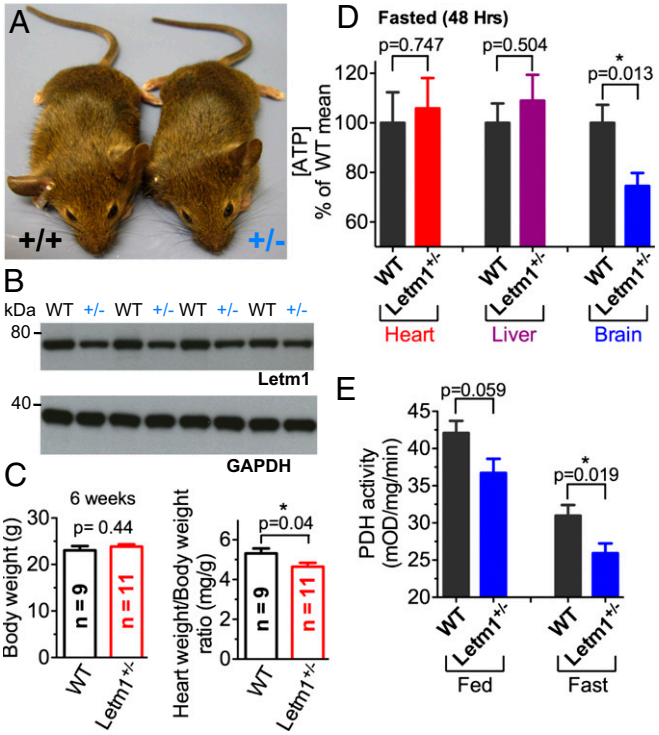

Fig. 4. Postembryonic development of *Letm1*$^{+/-}$ mice. (*A*) Representative images of 6-wk-old WT and *Letm1*$^{+/-}$ mice. (*B*) Letm1 levels in mouse brain tissues analyzed by Western blotting. (*C*) Body weight and heart/body weight ratio of WT and *Letm1*$^{+/-}$ mice (6 wk). (*D*) Among heart, liver, and brain ATP measurements in littermate-controlled WT and *Letm1*$^{+/-}$ male mice at 6 wk of age, only brain ATP levels fall in fasted mice. Tissue samples were collected from mice fasted for 48 h (n = 8–11). (*E*) Pyruvate dehydrogenase activity falls in brain tissues of fed or fasted mice (n = 6–12).

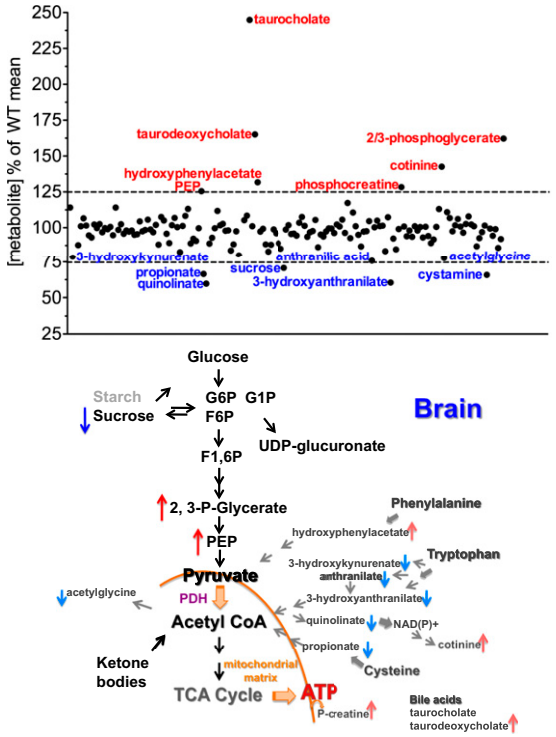

Fig. 5. Metabolic profile in brain samples from *Letm1*$^{+/-}$ mice. Normalized metabolite levels (LC-MS) of brain samples from littermate-controlled male WT (n = 9) and *Letm1*$^{+/-}$ (n = 8) mice at 6 wk of age under normal feeding conditions. The raw values of each metabolite were normalized by the mean values of those from the *wt* mice. F6P, fructose 6-phosphate; G1P, glucose 1-phosphate; G6P, glucose 6-phosphate; PDH, pyruvate dehydrogenase; PEP, phosphoenolpyruvate; TCA, tricarboxylic acid cycle; UDP, uridine diphosphate.

the most statistically significant metabolite reduction in liver samples from *Letm1*$^{+/-}$ fed mice was β-hydroxybutyrate (Fig. S4). During high carbohydrate intake, β-hydroxybutyrate is primarily synthesized in the liver from pyruvate-derived acetyl-CoA. During fasting, glucose and insulin levels drop, increasing fatty acid oxidation and greatly increasing fatty acid-derived acetyl-CoA. In turn, acetyl-CoA inhibits pyruvate dehydrogenase to limit glucose oxidation and to preserve glucose levels. In the present study, β-hydroxybutyrate levels were dramatically increased in both the liver and brain after fasting but to a similar extent in both *Letm1*$^{+/-}$ and WT mice (Fig. S4). The data suggest that the absence of Letm1 does not significantly affect fatty acid oxidation in mitochondria but it is important for pyruvate oxidation and glucose metabolism.

Letm1 Deficiency Increases Seizure Propensity. In humans, *Letm1* gene deletions are associated with seizures. In *Letm1*$^{+/-}$ mice, seizure activity increased when they were treated with kainic acid (Fig. S5), which through kainate receptors depolarizes neurons and increases intracellular Ca^{2+}. Initial seizure scores in *Letm1*$^{+/-}$ were ~1.5-fold higher than in WT mice (P = 0.03), with total scores increasing ~25% (P = 0.05; Fig. 6 *A* and *B*). In addition, brain, but not heart, [ATP] was reduced 25% (P = 0.04) in *Letm1*$^{+/-}$ mice after kainic acid treatment (Fig. 6*C*).

Taken together, these data suggest that reduced glucose, not fatty acid, oxidation accounts for the differential impact of tissue [ATP] in *Letm1*$^{+/-}$ mice. Reduced ketone body levels and altered tryptophan metabolism under normal feeding conditions may have broad effects on brain function (e.g., neuronal excitability and seizures) and development.

Discussion

Here we show that deleting the *Letm1* gene in mice is embryonically lethal before gastrulation (E6.5). We then investigated its function in heterozygotes, which mimics the situation in WHS, and found that reduction of Letm1 results in embryonic lethality in half of the mouse embryos, but those mice that survive are prone to seizures. This result is consistent with seizure phenotypes present in humans with WHS but does not explain the midline defects associated with that syndrome. These morphological defects are clearly explained by the loss of the *Whsc1* gene (ref. 17 and discussed below). We conclude that loss of Letm1 results in reduced glucose oxidation that preferentially affects glucose-dependent tissues such as neurons and developing tissues.

H^+ and Ca^{2+} are the key ions that create and gate the mitochondrial "battery" that provides the driving force for the F_1F_0 H^+-ATPase generation of ATP (4) and metabolite transport (18). In addition, increases in matrix [Ca^{2+}] stimulate dehydrogenases of the TCA cycle [e.g., pyruvate dehydrogenase (1)] and the F_1F_0 H^+-ATPase (2). Driven by large and fast changes in the cytoplasmic Ca^{2+}, the MCU provides large but self-limited (as $\Delta\Psi_{mito}$ collapses) pulses of matrix Ca^{2+}. In contrast, Letm1 as a Ca^{2+}/H^+ antiporter provides smaller and perhaps more localized changes in matrix Ca^{2+} while exporting H^+ crucial to the maintenance of the F_1F_0 H^+-ATPase. We hypothesize that Letm1 $Ca^{2+}{}_{mito}$ uptake is limited by $H^+{}_{mito}$ availability and the pH gradient across the IMM thus constrains $[Ca^{2+}]_{mito}$ increases mediated by Letm1. Our metabolic profiling studies and the seizure phenotype of *Letm1*$^{+/-}$ mice revealed that the primary impact of Letm1 loss (in mice that survive the fetal period) manifests as defects in glucose oxidation, consistent with Ca^{2+} regulation of TCA enzymes. One puzzling result from the metabolic

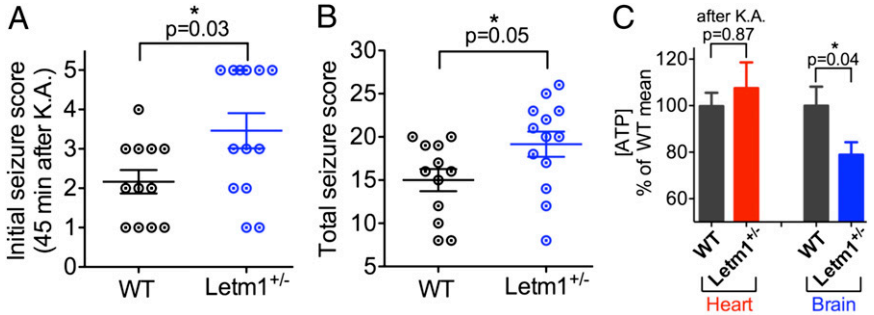

Fig. 6. Kainic acid induced seizures in *Letm1*$^{+/-}$ mice. (*A* and *B*) Littermate-controlled, 6-wk-old male WT (n = 12) and *Letm1*$^{+/-}$ mice (n = 13) injected i.p. with kainic acid (20 mg/kg). Racine scores of seizure-like activity were recorded every 15 min after kainic acid injection. Plots showing racine scores in the initial 45 min after injection (*A*) or the total cumulative scores (*B*). (*C*) Brain and heart [ATP] measurements were collected immediately after kainic acid treatment.

studies was the increase in phosphocreatine levels in *Letm1*$^{+/-}$ tissues. One possible explanation is that creatine kinase, localized between the mitochondrial outer and inner membranes and engaged in intracellular phosphotransfer networks (19), is somehow altered by pH or Ca^{2+} changes in this space.

The *Letm1* yeast homolog, *Mdm38*, was initially reported to be a mitochondrial K^+/H^+ exchanger that regulates mitochondrial volume (20). However, it seems highly unlikely that a K^+/H^+ exchanger could be a major regulator of mitochondrial volume. Cellular and mitochondrial [K^+] is ~150 mM, whereas matrix and cellular [H^+] is ~10–100 nM (~1 million-fold difference). Therefore, the H^+ gradient would have little impact on K^+ concentration, nor can it drive significant K^+ extrusion. For the same reason, the presence of a K^+/H^+ exchanger would eliminate any pH gradient and shortcut H^+ transport, which would be clearly detrimental to mitochondrial bioenergetics. In contrast, Ca^{2+} and H^+ are in comparable concentration ranges both inside and outside the matrix and a Ca^{2+}/H^+ exchanger would reasonably manage slow changes in cytoplasmic and matrix changes in these ions. RNAi-based Letm1 knockdown over long times in cultured cells resulted in proliferation arrest, but we interpret these effects to be more in line with complete loss of Letm1 and a plethora of secondary effects. Our previous recordings, reconstitution of purified Letm1 into liposomes, and current data support our conclusion that Letm1 primarily functions as a Ca^{2+}/H^+ antiporter.

We found that loss of Ca^{2+}/H^+ antiport predisposes mice to seizures, a key WHS phenotype in humans. Another gene frequently deleted in WHS, *Whsc1*, was systematically characterized in a *Whsc1* knockout mouse (17). *Whsc1*, one of five putative *Set2* homologs, governs H3K36 methylation along euchromatin by associating with the cell type-specific transcription factors Sall1, Sall4, and Nanog in embryonic stem cells, and Nkx2-5 in embryonic heart. *Whsc1*-deficient mice exhibit growth retardation and WHS-like midline defects, including congenital cardiovascular anomalies, and *Whsc1* haploinsufficiency phenotypes were exacerbated in *Nkx2-5* heterozygous mutant hearts. There are several key phenotypic differences between *Letm1* and *Whsc1* knockout mice. *Letm1*$^{-/-}$ mice died before E6.5 and nearly 50% of *Letm1*$^{+/-}$ mice died during early embryogenesis, whereas *Whsc1*$^{-/-}$ mice died in late embryonic stages or soon after birth. We hypothesize that there is a gene dosage effect of *Letm1* in early embryogenesis, perhaps due to cell cycle arrest. Whereas *Whsc1*$^{+/-}$ mice had WHS-like midline defects and altered cardiac functions, surviving *Letm1*$^{+/-}$ mice exhibited no obvious structural defects but had altered metabolic pathways, impaired control of brain [ATP], and seizures. Taken together, these results suggest that *Letm1* deficiency is related primarily to reduced brain function and seizures in WHS owing to impaired glucose oxidation and consequent cellular metabolic distortions.

Materials and Methods

Mouse Letm1 antibody was purchased from Proteintech (16024-1-AP), β-actin antibody from Sigma (A1978), human Letm1 antibody from Abcam (ab55434), GAPDH antibody from Cell Signaling (2118), and BrdU antibody from Abcam (ab6326). Kainic acid, oligomycin, trifluorocarbonylcyanide phenylhydrazone, rotenone, and antimycin were obtained from Sigma.

Letm1 Knockout Mice. Mice lacking functional Letm1 protein were derived from the BayGenomics gene trap of the *Letm1* locus (DD0926 and CC0204). The exogenous gene-trap vector sequence, containing an in-frame splice acceptor site followed by coding sequence for a β-galactosidase/neomycin (β-Geo) fusion protein, was inserted into introns following exon 1 (DD0926) or exon 3 (CC0204). The insertion of a trapping vector after exon 1 or exon 3 of *Letm1* creates fusion transcripts and premature stop codons, thus preventing the synthesis of full-length mRNA. Chimeric male mice were derived from sequence-verified gene-trap embryonic stem cells and used to establish heterozygous founder mice. *Letm1*$^{+/-}$ mice were then backcrossed against *wt* SvEv129 for 5–10 generations.

Male littermate-controlled *Letm1*$^{+/-}$ and WT mice from the two independent gene-trap lines were used in a similar ratio in most of the experiments, including tissue [ATP], metabolite measurements, and seizure experiments. For timed matings of *Letm1*$^{+/-}$ intercrosses, mice were examined every morning for vaginal plugs. Detection of a vaginal plug was defined as E0.5. Females were killed at E6.5 and at specific embryonic days. Embryos were dissected from the uteri; the uteri were examined for evidence of fetal resorption and genotyped. All animal husbandry and experimental procedures were approved by, and performed in accordance with, the guidelines of the Children's Hospital Boston Institutional Animal Care and Use Committee.

Mouse Genotyping. The genomic locus of the Bay Genomics gene-trap vector insertion was identified by PCR using a series of forward primers spaced at 1- to 2-kb intervals in the predicted intronic *Letm1* sequence, along with a β-*Geo*–specific reverse primer to amplify a product containing the β-*Geo* insertion site. Genotypes were confirmed by triplex PCR performed on genomic DNA isolated from mouse tails using gene-specific primers: DD0926_Forward primer: 5′- CCA GCT AGA GGC TGG GTT CTT GTT - 3′; DD0926_Reverse primer-1: 5′- GGG TTC GTG TCC TAC AAC ACA CAC TC - 3′; DD0926_Reverse primer-2: 5′- TGG TTG TTC CCT CAC CAC CAT AAG C - 3′; CC0204_Forward primer: 5′- CCA GGC ACA CAT GTA CCC TTA CA - 3′; CC0204_Reverse primer-1: 5′- GCC AGT GAG GCT TCT AGG ACA AGA G - 3′; CC0204_Reverse primer-2: 5′- ACA CAA CAG CCC AGT TGT CGG CTA - 3′.

ATP Measurements in Cultured Cells. ATP levels were measured with luciferase in cultured cells or tissue samples (ATPlite assay kit; Perkin-Elmer).

Primary Culture of Embryonic Fibroblasts. Mouse embryonic fibroblasts were isolated from E13.5 embryos and grown in a mixture of DMEM and F12 medium. Cells were split at a 1:3 ratio when they reached confluence. Adenoviruses expressing pericam were used for infection. All experiments were done within three passages from initial isolation.

Measurement of O_2 Consumption Rate. Oxygen consumption rate in cultured embryonic fibroblasts was measured using a Seahorse XF-24 analyzer according to the manufacturer's standard protocol. Cells were seeded to achieve ~70% confluence at the time of measurement and incubated in low-pH buffered DMEM for 1 h before the assay. WT and *Letm1*$^{+/-}$ fibroblasts were seeded to achieve similar cell number at the time of measurements and were again counted after the measurement.

Quantification of Mitochondrial Morphology. Mitochondrial morphology in cultured cells was quantified using a modified ImageJ macro as described previously (21). Mitochondria stained with TMRM were extracted to gray-scale, inverted to show mitochondrial fluorescence as black pixels, thresholded to optimally resolve individual mitochondria, and mitochondrial outlines were traced. Mitochondrial area and perimeter were then measured and plotted.

Pyruvate Dehydrogenase Activity Assay. Pyruvate dehydrogenase activity from brain tissues was measured using a microplate assay kit (Mitosciences) with slight modifications. Briefly, mitochondria were collected by homogenizing tissues in isolation buffer [250 mM sucrose, 50 mM KCl, 5 mM Hepes, 1 mM EGTA, 2% (wt/vol) BSA, 1mM dithioerythritol (DTE), 20 mM Na^+-dichloroacetate, phosphatase and protease inhibitor mixtures, pH 7.2]. Mitochondrial fractions were then solubilized (0.5% Triton X-100, 20 mM Tris·Cl, 50 mM NaCl, 0.5 mM EGTA, 5 mM $MgCl_2$, 1 mM DTE, 10 mM Na^+-dichloroacetate, phosphatase and protease inhibitor mixtures, pH 7.4). Pyruvate dehydrogenases from the mitochondrial lysate (400 μg) were placed in the microplate reader and activity assays conducted according to the manufacturer's protocol.

Extraction of Tissue Metabolites and Tissue ATP Measurements. Mouse tissues were collected (100 mg), snap-frozen in liquid nitrogen, and homogenized in 80% methanol (1 mL). The homogenate was then centrifuged at 4 °C for 10 min at 14,000 × *g*. Supernatants were transferred into an O-ring tube and stored at −80 °C for LC-MS–based metabolite measurements. For ATP measurements, 10-μL sample extracts were dried in 96-well plates under a gentle N_2 stream then immediately measured using the ATPlite assay kit.

Metabolic Profiling. Profiles of endogenous, water-soluble metabolites were obtained using targeted LC-MS methods operating in positive and negative ionization modes. Both methods were developed using reference standards of each metabolite to determine chromatographic retention times and

MS multiple reaction monitoring transitions, declustering potentials, and collision energies. Negative ionization mode data were acquired using an ACQUITY UPLC (Waters) coupled to a 5500 QTRAP triple quadrupole mass spectrometer (AB SCIEX). Tissue extracts (10 μL) were injected onto a 150- × 2.0-mm Luna NH2 column (Phenomenex) that was eluted at a flow rate of 400 μL/min with initial conditions of 10% mobile phase A (20 mM ammonium acetate and 20 mM ammonium hydroxide in water) and 90% mobile phase B (10 mM ammonium hydroxide in 75:25 vol/vol acetonitrile/methanol) followed by a 10-min linear gradient to 100% mobile phase A. The ion spray voltage was −4.5 kV and the source temperature was 500 °C. Positive ionization mode data were acquired using a 4000 QTRAP triple quadrupole mass spectrometer (AB SCIEX) coupled to an 1100 Series pump (Agilent) and an HTS PAL autosampler (Leap Technologies). Tissue extracts were diluted using nine volumes of 74.9:24.9:0.2 (vol/vol/vol) acetonitrile/methanol/formic acid containing stable isotope-labeled internal standards (valine-d8; Isotec and phenylalanine-d8; Cambridge Isotope Laboratories). The samples (10 μL) were injected onto a 150- × 2.1-mm Atlantis HILIC column (Waters). The column was eluted isocratically at a flow rate of 250 μL/min with 5% mobile phase A (10 mM ammonium formate and 0.1% formic acid in water) for 1 min followed by a linear gradient to 40% mobile phase B (acetonitrile with 0.1% formic acid) over 10 min. The ion spray voltage was 4.5 kV and the source temperature was 450 °C. Data were analyzed using MultiQuant software (AB SCIEX).

Kainic Acid-Induced Seizure Test. Littermate-controlled male mice (6 wk old) were injected with kainic acid (20 mg/kg in phosphate-buffered solution at 5 mg/mL) via i.p. injection. Mice were observed for 2 h following injection and scored for seizure-like activity according to the Racine scoring system; the experimenters were blind to genotype. Brain and heart tissues from these mice were then immediately collected, snap-frozen in liquid nitrogen, and homogenized in 80% methanol for ATP measurements.

Histology and Immunohistochemistry. Embryos were collected in PBS on ice and fixed in 4% paraformaldehyde at 4 °C for 2 h. After washing in PBS, tissues were treated sequentially with 15% and 30% sucrose until the tissue had been fully penetrated, embedded in Optimal Cutting Temperature compound (Tissue-Tek), and snap-frozen. Cryosections (10–12 μm) were collected on positively charged slides. Tissues were blocked with PBS supplemented with 0.1% Triton X-100 and 5% normal donkey serum for 1 h at room temperature, followed by first antibody incubation at 4 °C overnight. Signals were developed with Alexa-conjugated secondary antibodies (Invitrogen). Images were acquired on an FV1000 confocal microscope (for fluorescence staining) or Nikon Eclipse 80i microscope (for embryos). Proliferating cells were analyzed by incorporation of BrdU (i.p. injection, 1 h before dissection). After fixation, BrdU was detected by treating cells with 2 M HCl at 37 °C for 30 min followed by staining with BrdU antibody. Apoptosis was detected with the In Situ Cell Death Detection Kit (TUNEL; Roche).

Inductively Coupled Plasma-MS For inductively coupled plasma (ICP)-MS, tissue samples were digested with 1% HNO_3 (95 °C, 4 h). Triplicate samples were diluted and analyzed by ICP-MS in the Department of Earth and Planetary Sciences at Harvard University; total K^+ and Na^+ were measured.

Mitochondrial-Targeted-Pericam Stable Cell Lines and RNAi in Mammalian Cells. Stable, inducible Flp-In-293-pericam cell lines were generated as previously described (12). siRNAs against human Letm1 and control siRNAs were purchased from Ambion. Flp-In 293 cells split at ∼25% confluence were transfected with siRNAs (50 μM) using Lipofectamine RNAiMAX (Invitrogen), incubated for 48 h, and transfected again at ∼25% confluence for another 42–48 h before experiments. Sense sequence for Letm1-siRNA#1: UCCACAUUUGAGACUCAGUtt; Letm1-siRNA#2: AUGUUCCAUUUGGCUGCUGtt.

$[Ca^{2+}]_{mito}$, $[H^+]_{mito}$, and $\Delta\Psi_{mito}$ Measurements. Fluorescence measurements of cells expressing mitochondrial-targeted (mt)-pericam were made using a FluoView 1000 confocal microscope (Olympus). For experiments with permeabilized cells, 100 μM digitonin was applied for 60 s followed by 10-min perfusion in intracellular solution (140 mM KCl, 5 mM succinate, 20 mM Hepes, 0.5 mM EGTA, pH 7.2). The experiments were performed in intracellular medium with $[Ca^{2+}]$ as indicated. $[Ca^{2+}]_{mito}$ and $[H^+]_{mito}$ were monitored at 405 nm and 488 nm excitation wavelengths, respectively, and emission was collected at 500–510nm for $[Ca^{2+}]_{mito}$ and 510–535 nm for $[H^+]_{mito}$. $\Delta\Psi_{mito}$ was measured using TMRM (Molecular Probes). Cells were loaded with 10 nM TMRM (for mammalian cells) for 10 min and the fluorescence levels (580 nm) measured from 545 nm excitation wavelengths.

Statistics. All values shown are means ± SEM unless indicated otherwise. Bar graphs and statistics were generated using Prism (GraphPad). The *P* values shown were calculated using Student's *t* test (two-tailed, unpaired).

ACKNOWLEDGMENTS. We thank Robert Gerszten, Kerry Pierce, Amanda Souza, and Lee Roberts for performing metabolic profiling assays and Adrian Padilla for scoring the seizure activities in mice. D.J. is a recipient of fellowship awards from the Canadian Institutes of Health Research and the Alberta Heritage Foundation for Medical Research.

1. Denton RM (2009) Regulation of mitochondrial dehydrogenases by calcium ions. *Biochim Biophys Acta* 1787(11):1309–1316.
2. Balaban RS (2009) The role of Ca^{2+} signaling in the coordination of mitochondrial ATP production with cardiac work. *Biochim Biophys Acta* 1787(11):1334–1341.
3. Szabadkai G, Duchen MR (2008) Mitochondria: The hub of cellular Ca^{2+} signaling. *Physiology (Bethesda)* 23:84–94.
4. Nicholls DG (2005) Mitochondria and calcium signaling. *Cell Calcium* 38(3-4):311–317.
5. Rizzuto R, Pozzan T (2006) Microdomains of intracellular Ca^{2+}: Molecular determinants and functional consequences. *Physiol Rev* 86(1):369–408.
6. Kirichok Y, Krapivinsky G, Clapham DE (2004) The mitochondrial calcium uniporter is a highly selective ion channel. *Nature* 427(6972):360–364.
7. De Stefani D, Raffaello A, Teardo E, Szabò I, Rizzuto R (2011) A forty-kilodalton protein of the inner membrane is the mitochondrial calcium uniporter. *Nature* 476(7360):336–340.
8. Baughman JM, et al. (2011) Integrative genomics identifies MCU as an essential component of the mitochondrial calcium uniporter. *Nature* 476(7360):341–345.
9. Bernardi P (1999) Mitochondrial transport of cations: Channels, exchangers, and permeability transition. *Physiol Rev* 79(4):1127–1155.
10. Gunter TE, Yule DI, Gunter KK, Eliseev RA, Salter JD (2004) Calcium and mitochondria. *FEBS Lett* 567(1):96–102.
11. Csordas G, Varnai P, Golenar T, Sheu SS, Hajnoczky G (2011) Calcium transport across the inner mitochondrial membrane: Molecular mechanisms and pharmacology. *Mol Cell Endocrinol* 22:22.
12. Jiang D, Zhao L, Clapham DE (2009) Genome-wide RNAi screen identifies Letm1 as a mitochondrial Ca^{2+}/H^+ antiporter. *Science* 326(5949):144–147.
13. Bergemann AD, Cole F, Hirschhorn K (2005) The etiology of Wolf-Hirschhorn syndrome. *Trends Genet* 21(3):188–195.
14. Wallace DC, Fan W (2009) The pathophysiology of mitochondrial disease as modeled in the mouse. *Genes Dev* 23(15):1714–1736.
15. Wang TJ, et al. (2011) Metabolite profiles and the risk of developing diabetes. *Nat Med* 17(4):448–453.
16. Finley LW, et al. (2011) SIRT3 opposes reprogramming of cancer cell metabolism through HIF1α destabilization. *Cancer Cell* 19(3):416–428.
17. Nimura K, et al. (2009) A histone H3 lysine 36 trimethyltransferase links Nkx2-5 to Wolf-Hirschhorn syndrome. *Nature* 460(7252):287–291.
18. Halestrap AP (1978) Pyruvate and ketone-body transport across the mitochondrial membrane. Exchange properties, pH-dependence and mechanism of the carrier. *Biochem J* 172(3):377–387.
19. Dzeja PP, Terzic A (2003) Phosphotransfer networks and cellular energetics. *J Exp Biol* 206(Pt 12):2039–2047.
20. Nowikovsky K, et al. (2004) The LETM1/YOL027 gene family encodes a factor of the mitochondrial K^+ homeostasis with a potential role in the Wolf-Hirschhorn syndrome. *J Biol Chem* 279(29):30307–30315.
21. Dagda RK, et al. (2009) Loss of PINK1 function promotes mitophagy through effects on oxidative stress and mitochondrial fission. *J Biol Chem* 284(20):13843–13855.